

IET Renewable Power Generation

Special Issue Call for Papers

**Be Seen. Be Cited.
Submit your work to a new
IET special issue**

Connect with researchers and
experts in your field and
share knowledge.


Be part of the latest research
trends, faster.

[Read more](#)



The Institution of
Engineering and Technology

Analysis and wave tank verification of the performance of point absorber WECs with different configurations

Xiaofan Li¹  | Dillon Martin¹ | Boxi Jiang¹ | Shuo Chen¹ | Krish Thiagarajan^{2,*} | Robert G. Parker³ | Lei Zuo¹

¹ Department of Mechanical Engineering, Virginia Tech, Blacksburg, Virginia 24061, USA

² Advanced Structures and Composites Center, University of Maine, Orono, Maine 04469, USA

³ Department of Mechanical Engineering, University of Utah, Salt Lake City, Utah 84112, USA

Correspondence

Lei Zuo, 315 Durham Hall, Blacksburg, Virginia 24061, USA.

Email: leizuo@vt.edu

* Present address

Krish Thiagarajan Sharman, Department of Mechanical and Industrial Engineering, University of Massachusetts Amherst, Amherst, Massachusetts, USA.

Funding information

U.S. Department of Energy EERE, Grant/Award Number: DE-EE0007174; European Union Horizon 2020 Framework Programme, Grant/Award Number: H2020

Abstract

Extracting energy from ocean waves has become a heated topic since the energy crisis of the 2000s. Among all the different concepts and designs of Wave Energy Converter (WEC), point absorber is a widely adopted type with great potential, and various configurations and constraints are applicable to it. Here, the point absorber WECs with four different set-up configurations are explored: single body heaving WEC, two-body heaving WEC, two-body WEC with a flat plate (Reference Model 3), and a two-body WEC with a cylinder-shaped second body. Dynamic models are established for each case and wave tank tests are conducted for verification. The results show that the power capture of a point absorber can benefit from several aspects: the two-body WEC with a streamlined shape can double the wave capture width ratio (up to 66.5%) over the single-body WEC or Reference Model 3, while coupling other motion or mooring dynamics can further improve the capture width ratio by 12% by increasing the relative motion stroke.

1 | INTRODUCTION

The overall assessment of the wave energy potential is about 3.7 TW globally [1], which is in the same order as the world energy consumption [2]. In addition, extracting ocean wave energy not only can relieve the tension of increasing world energy demand, it can also benefit the environment as clean renewable energy [3]. Different concepts and designs of wave energy converters (WECs) have been proposed and developed over the past two centuries, especially after the 1970 and 2000 global energy crises. Among those WECs, a point absorber, which uses heave oscillations caused by a wave to extract energy, is one of the most widely adopted concepts for ocean wave energy conversion. In 1975, Budal and Falnes proposed the concept of harvesting ocean wave energy through a point absorber [4]. The idea was soon brought to the interest of many researchers and much

profound theoretical work for feasibility and optimization was done. In 1976, Evans [5] and Mei [6] calculated the maximum power absorption of the single body point absorber, showing that it can be achieved through the resonant approach, which means to match the natural frequency of the buoy with the wave frequency. Investigations on the single body point absorber were made by multiple researchers. For example, Eriksson analyzed a single body point absorber with a linear direct-drive PTO and validated through in-water experiment at Lysekil [7]. AWS adopted a submerged design and tested the concept in 2004 in Portugal [8]. Vicente, Falcao and Justino analyzed the non-linear dynamics for a moored point absorber [9]. Wang et al. attempted to improve the power absorption through electric load control [10]. Liu and Pastor conducted a series of research using both time domain and frequency domain approach to optimize the output power for the point absorber [11–13]. Guo

This is an open access article under the terms of the [Creative Commons Attribution License](https://creativecommons.org/licenses/by/4.0/), which permits use, distribution and reproduction in any medium, provided the original work is properly cited.

© 2021 The Authors. *IET Renewable Power Generation* published by John Wiley & Sons Ltd on behalf of The Institution of Engineering and Technology

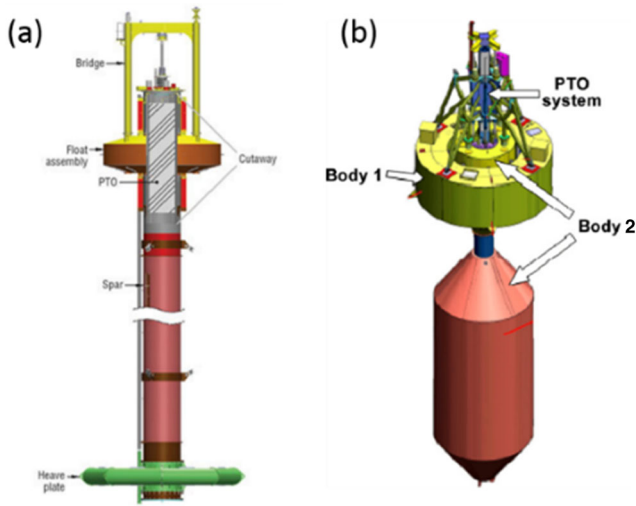


FIGURE 1 Two-body point absorbers with different submerged reactive body shape (a) Flap heave plate shape; (b) Streamlined cone shape

et al. tested a point absorber with the non-linear forces taken into consideration and achieved good matching results [14]. In real applications, however, the frequency of ocean wave can be low to the level of 0.1 Hz, leading to an extremely large physical structure of the point absorber which can be counted as uneconomic and non-feasible [15]. Moreover, single body point absorbers have a high demand for supporting infrastructures to have a relative motion, which leads to higher cost.

A variety of ideas was raised to overcome the disadvantages of single body point-absorbers and different configurations were adopted for improving their performance. Among those ideas, the most common approach is to design a reactive body, which can have relative motion with the floating buoy. The advantage of having a reactive body is in several aspects. For example, the natural frequency of the overall system can be adjusted to match the dominant wave frequency by tuning the second body and it has less demand for support infrastructures [16]. As a result, many two-body point absorber prototypes were built and tested. Among them, the design of the second body has two popular options. One is a flat heave plate, which gives a large added mass which is shown in Figure 1(a), as adopted in the PowerBuoy developed by Ocean Power Technologies Inc. and in Sandia National Lab's Reference Model Project (RMP) [17, 18]. Another common design of the reactive body is a cylinder shape with cones to reduce the viscous damping, as in the prototypes built and tested by the WaveBob at multiple sites in different scales as illustrated in Figure 1(b) [19]. The selection of different second body shapes brings different dynamics to the system resulting in different performances. Beatty et al., conducted an experiment on these two shapes for the second body in regular waves, it is found that the heave plate shape second body has a large radiated wave force and it is more likely to be influenced by the viscous damping, whereas the streamlined shape design has the opposite [20]. Dillon et al. analyzed the influence of three body shapes using the numerical simulation in both time domain and frequency domain [21]. Xu et al. studied a two-body point absorber similar to the RM3 point absorber and

verified the performance in wave tank [22]. In addition, multiple pieces of literature exist for optimizing the power absorption for the point absorbers through control approaches [23–25]. However, previous studies are usually conducted with only heaving motion in consideration, where the influence of other motions (like surge/sway and pitch/roll) and mooring dynamics are not included. Moreover, the non-linear viscous damping and PTO forces are either simplified or not included in the study. Therefore, a comprehensive study and experiment validation are still necessary.

In this paper, point absorber WECs with four configurations are studied. Firstly, a single body heaving-only configuration is selected as the baseline of the study. This is compared with a two-body heaving-only configuration to investigate the advantages of the latter. Two moored configurations of the two-body point absorber that adopt different second body designs are also investigated. Through numerical study and wave tank validation, the following research findings are revealed. Firstly, the two-body design can achieve the frequency tuning effect. Secondly, the relative heave motion between the two bodies can be boosted from the motions of other degrees of freedom (DoF). Lastly, the streamlined second body design (cylinder-cone shape) can achieve higher optimum power. The rest of the paper is organized as follows. In Section 2, the four different configurations are introduced and their dynamic modelling is established. In Section 3, the detailed setup of wave tank tests is introduced. In Section 4, the test results and the numerical simulation results are presented to validate the major findings of this paper. The conclusions are given in Section 5.

2 | TEST CONFIGURATIONS AND MODELLING

Figure 2 shows the four configurations discussed in this paper. They are constrained differently. Configuration (a) is a single body WEC; configuration (b) is guided to allow heave motions of the two bodies; configurations (c) and (d) are constrained with three-point moorings.

The typical design for a single body point absorber is illustrated in Figure 2(a), where a floating buoy moves along the incident wave. The buoy is guided by a rigid structure where in the figure is represented by a column. The buoy moves along the structure and is constrained to the heave only direction, thus only one DoF of motion needs to be taken into consideration. The motion of the buoy is then adopted to drive the power take-off (PTO) and generate electricity.

For the single body point absorber, the equation of motion can be obtained as:

$$m_1 \ddot{z}_1 = f_{e,b}^1 + f_{pto}^1 + f_{hs,b}^1 + f_{r,b}^1 + f_{v,b}^1 \quad (1)$$

where

- m_1 is the mass of the floating buoy
- \ddot{z}_1 is the acceleration of the buoy in heave motion

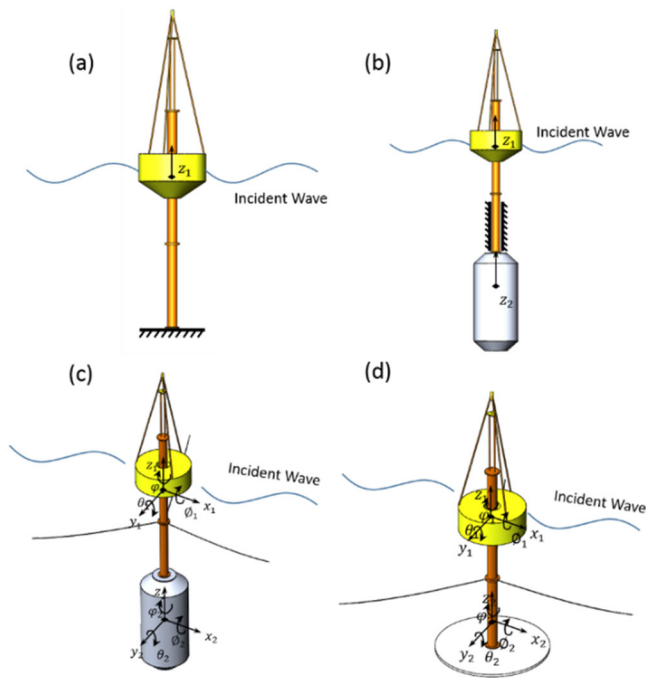


FIGURE 2 Scheme of the configurations considered in this study and tested in a wave tank

- $f_{e,b}^1$ is the heave direction excitation force cast on the buoy from the wave
- f_{pto} is the force from the PTO system
- $f_{bs,b}^1$ is the hydrostatic restoring force in heave
- $f_{r,b}^1$ is the radiation wave induced force in heave
- $f_{v,b}^1$ is the viscous force in heave

The PTO adopted in the design is based on the Mechanical Motion Rectifying (MMR) mechanism, which brings in a unique dynamic property of piecewise non-linear PTO force. The detailed introduction to the PTO can be found in existing literature [26]. The MMR mechanism can rectify the motion of the PTO by introducing the status of engagement and disengagement based on its input and output speed, the dynamic force from the PTO can be presented as:

$$f_{pto} = \begin{cases} -m_e \ddot{\chi}_1 - c_e \dot{\chi}_1 - f_f & \text{if engaged} \\ -f_f & \text{if disengaged} \end{cases} \quad (2)$$

where m_e is the equivalent mass of the PTO, c_e is the equivalent damping of the PTO, and the friction force f_f can be presented as [27]:

$$f_f = \begin{cases} f_c + (f_s - f_c) e^{\left(\frac{-v}{v_s}\right)^2} + c_v v & \text{if } v \neq 0 \\ f_e & \text{if } v = 0 \end{cases} \quad (3)$$

Here,

- f_f is the total friction force applied on the PTO

- f_c is the Coulomb friction force
- f_s is the Stribeck friction force
- f_e is the static friction force
- v and v_s are the velocity of the PTO and the relative velocity threshold for the Stribeck friction

Since both the MMR mechanism and the friction can lead to non-linear dynamics, the force induced by the radiated wave can be described using the Cummins equation [28]:

$$f_{r,b}^1 = -A_1(\infty) \ddot{\chi}_1 - \int_{-\infty}^t k_1(t-\tau) \dot{\chi}_1(\tau) d\tau \quad (4)$$

$$k_1(t) = \frac{2}{\pi} \int_0^\infty b_1(\omega) \cos \omega t d\omega$$

where

- $A_1(\infty)(i, j = 1, 2)$ is the added mass when the frequency approaches to infinity
- $b_1(\omega)$ is the frequency dependent radiation damping

Both unknown terms can be acquired using linear potential wave theory and the Boundary Element Method (BEM), and they can be calculated by multiple commercial or open-source software packages.

The viscous induced drag force is not considered in the hydrodynamic parameters acquired from the linear wave theory. As a result, a quadratic drag damping term is added to the dynamic model and can be extended as:

$$f_{v,b}^1 = -\frac{1}{2} \rho c_{d1} A_{c1} (\dot{\chi}_1 - v_b) |\dot{\chi}_1 - v_b| \quad (5)$$

where

- ρ is the density of the ocean water
- c_{d1} is the drag coefficients, which depends on the geometric shapes of the bodies
- A_{c1} is the characteristic areas for the floating buoy, which is the orthographic projection of the floater on a plane perpendicular to the direction of motion
- v_b is the flow velocity relative to the floater

From the equations above, a high-fidelity time domain model can be established for simulating the performance of the single body point absorber using the numerical approach, which is also used for simulating the other configurations. The explicit analysis and experimental verification is achieved and the results show that the dynamic model can accurately predict the performance of the point absorber [29].

As illustrated in Figure 2(b), the two-body, heave-only wave energy point absorber consists of one floating buoy and a neutrally buoyant submerged body. For the case in the figure, the column is constrained against all rotary, surge and sway motions to simplify the dynamic analysis as heave motion only. Energy is absorbed through the relative heave motion between the two

bodies, with both bodies constrained to have heave motion only. It is modelled as a 2DOF system, where only \tilde{z}_1 and \tilde{z}_2 , is considered. It is worthy to note that the simplified model with only 2DOF is widely used in the literature regardless of the adopted constraint.

For the heave only two-body point absorber, the equation of motion can be obtained as:

$$\begin{aligned} m_1 \ddot{\tilde{z}}_1 &= f_{e,b}^1 + f_{pto}^1 + f_{hs,b}^1 + f_{r,b}^1 + f_{v,b}^1 \\ m_2 \ddot{\tilde{z}}_2 &= f_{e,b}^2 - f_{pto}^2 + f_{hs,b}^2 + f_{r,b}^2 + f_{v,b}^2 \end{aligned} \quad (6)$$

Here, the nomenclature is similar to Equation (1) but subscripts ($i = 1, 2$) representing the forces applied to the floating body and the submerged body respectively. Since the distance between the two bodies is large, the force from the other body induced radiated wave is not considered here to simplify the simulation.

Here, the PTO force is related to the relative motion and can be presented as:

$$f_{pto} = \begin{cases} -m_e (\ddot{\tilde{z}}_1 - \ddot{\tilde{z}}_2) - c_e (\dot{\tilde{z}}_1 - \dot{\tilde{z}}_2) - f_f & \text{if engaged} \\ -f_f & \text{if disengaged} \end{cases} \quad (7)$$

Figure 2(c) and (d) show typical mooring configurations for the two-body point absorbers, where the submerged second bodies have different shapes. The energy abstraction remains come from the relative motion between the \tilde{z}_1 and \tilde{z}_2 and can be boosted from the other motions including the pitch and surge. The individual body is free to move in all DOF and the mooring lines will provide soft constrain to the system. The $x_1, y_1, \tilde{z}_1, \theta_1, \theta_1$ and φ_1 each represents the surge, sway, heave, pitch, roll and yaw motion of the floating body. Similarly, the $x_2, y_2, \tilde{z}_2, \theta_2, \theta_2$ and φ_2 each represent motions of the submerged body respectively.

Assuming the incident wave interacting with the point absorber has constant direction, the cross-fluid sway, roll and yaw motions for both bodies will be relatively small compared to the other motions. As a result, they are ignored and only the heave \tilde{z} , surge x , and pitch motions of the two bodies are considered. In addition, a linear guide system is assembled between the two bodies that only allows relative heave motion such that,

$$\theta_1 = \theta_2 \quad (8)$$

As a result, considering that the relative heave motion is small compared to the overall scale, the two bodies can be regarded as a single body for modelling the motion. By combining two bodies as one, the motion for the two bodies in the pitch and surge motion can be modelled as:

$$\begin{aligned} m_c \ddot{x}_c &= f_{e,s}^c + f_{hs,s}^c + f_{r,s}^c + f_{v,s}^c + f_{m,s}^c \\ J_c \ddot{\theta}_c &= T_{e,p}^c + T_{hs,p}^c + T_{r,p}^c + T_{v,p}^c + T_{m,p}^c \end{aligned} \quad (9)$$

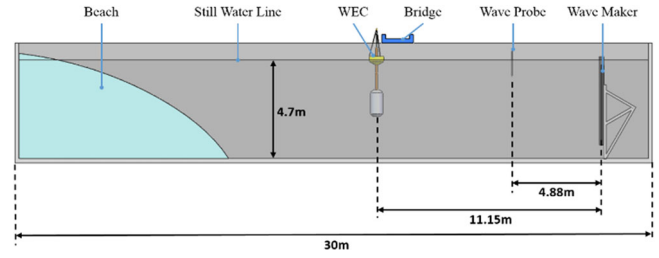


FIGURE 3 Scheme of the configurations tested in the wave tank

where

- J_c and m_c are the combined rotary inertia and mass of the two bodies when the floating buoy is located at equilibrium position
- $T_{e,p}^c$ and $f_{e,s}^c$ are the excitation torque and force on the combined body in pitch and surge
- $T_{hs,p}^c$ and $f_{hs,s}^c$ are the hydrostatic torque and force on the combined body in pitch and surge
- $T_{r,p}^c$ and $f_{r,s}^c$ are the radiation force on the combined body in pitch and surge
- $T_{v,p}^c$ and $f_{v,s}^c$ the viscous induced torque and force on the combined body in pitch and surge
- $T_{m,p}^c$ and $f_{m,s}^c$ the mooring induced force on the combined body in pitch and surge

Since the mooring set-up used in this paper is by fishing line and springs, the mooring induced force and torque can be simplified as:

$$\begin{aligned} f_{m,s}^c &= -k_m x_c \\ T_{m,p}^c &= -f_{m,s}^c d_{gc} \end{aligned} \quad (10)$$

here

- k_m is the combined stiffness in the surge motion from all mooring lines
- d_{gc} is the distance between the mooring point to the center of gravity of the combined bodies

However, since the mooring line is designed to be close to the gravity center, the mooring-induced torque is small and can be neglected in this study.

3 | WAVE TANK TEST SET-UP

With the four different configurations introduced, prototypes were assembled and tested in the wave tank at the Alford W2 Ocean Engineering Lab at the University of Maine and the BGO FIRST facility operated by OCEANIDE. The general test configuration is illustrated in Figure 3. The prototype used during the tests is scaled down to fit into the wave tank and keep the influence of sidewalls to a minimum. Moreover, the beach at the end of the wave tank is designed with a porous surface

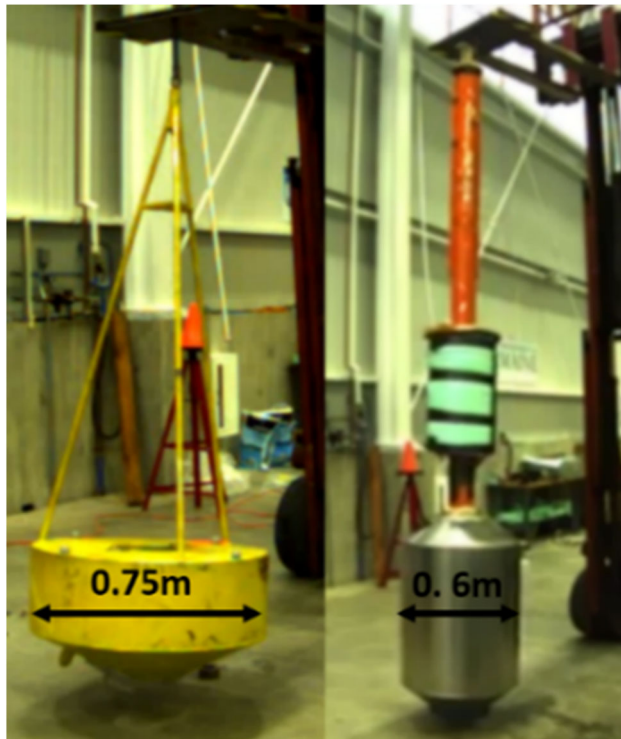


FIGURE 4 Pre-test on the mass property of the bodies

to minimize the influence of the reflected wave. As a result, the incident wave will be dominant. The waves at the location of the model were calibrated with a wave probe prior to the installation of the model. Wave probes are used during the test to monitor the wave height during the tests. As an ISO-certified facility, the experimental procedures were standardized and all wave data checked to guarantee that they are all within the acceptable margins of error. A bridge over the tank having high structural stiffness is used as the ground for the mounting constraint for configurations (a) and (b). Figure 3 illustrates the setup of the tests in the Alford W2 Ocean Engineering Lab.

The body mass properties are tested ahead of the wave test. Figure 4 describes the suspension and swing-test procedures used to measure the center of gravity and moment of inertia for the buoy and the second body. The diameters of the floating buoy and the submerged tank are shown in the figure as well. Other properties including the moment of inertia in different directions are obtained through the test as well. Foam is added to adjust the buoyancy of the designed submerged body so it can achieve the status of neutrally buoyed at the desired position of the free surface. The basic parameters and dimensions are listed in Table 1. In addition, free decay tests were also conducted to identify the viscous caused drag damping coefficient, which is used in the dynamic model for simulation. Through the preliminary test of the mass property and free decay. The unknown and unverified physical parameters of the prototype are obtained. These parameters are input to the dynamic model of the prototype, thus the model is refined and can achieve better simulation accuracy.

TABLE 1 The basic parameters for the two-body WECs with cylinder-cone shaped submerged body

	Floater	Submerged body
Dry mass (kg)	60.1	336.4
Diameter (m)	0.75	0.6
Height (m)	1.2	2.6

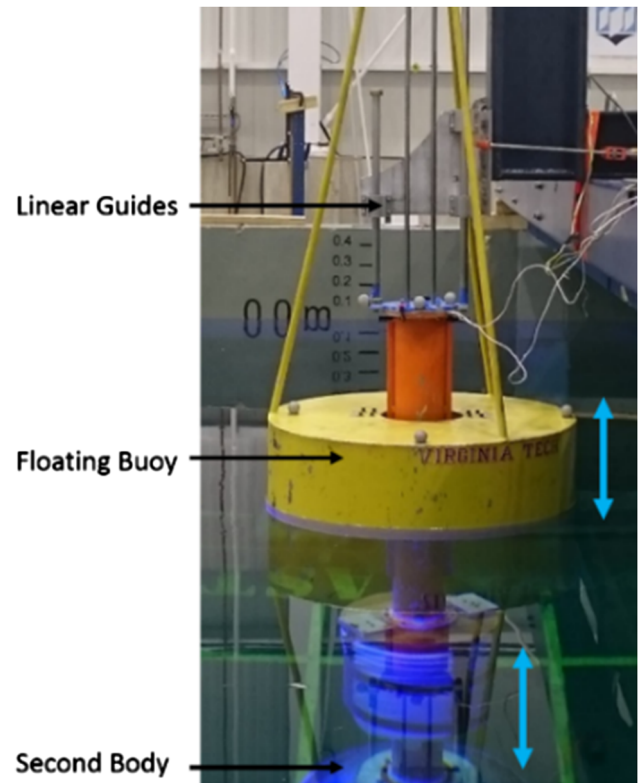


FIGURE 5 Test set-up for the two-body heave only configuration, blue arrows indicate the motion of either body

In the heave-only tests, the floating buoy motion is constrained to the submerged body through a linear guide system, whereas the motion of the submerged body is constrained with the bridge. Figure 5 shows the heave-only test setup for the two-body point absorber, which constrains the motions of both bodies to be in the heave direction only.

For the two-body moored configuration, the three mooring lines are attached close to the CG with an angle of 120° between each other, which is shown in Figure 6. The rear end mooring lines are connected to the anchor point on the wave tank through a spring with the stiffness of 40 N/m.

The measurement sensors of the experiment are listed in Table 2. For the wave height measurement, two wave probes are deployed between the wave paddles and the prototype to ensure and measure the properties of the incident wave (Figure 3). A load cell is mounted between the floating buoy and the PTO column to measure the PTO force, and a string potentiometer is used to measure the displacement of the

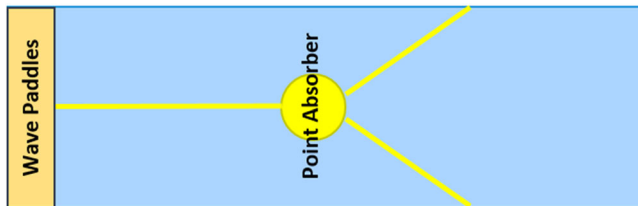


FIGURE 6 Scheme for the two-body point absorber moored configuration set-up

TABLE 2 The list of sensors used in the wave tank test

Sensor	Measurement (Unit)
Load cell	PTO force (N)
String pot	PTO displacement (m)
Wave prob1	Incident wave height (m)
Wave prob2	Incident wave height (m)
Qualisys motion capture system	Body motion in all DOF (m/°)
Oscilloscope	Generator voltage output (V)
Hall effect current sensor	Generator current output (A)

PTO. An oscilloscope is used to monitor the voltage output from the generator, and the current output of the generator is detected by a Hall Effect current sensor. The motion of both the floating buoy and the submerged body are monitored by a Qualisys motion capture system. All sensing signals are transmitted to a multi-channel DAQ system to guarantee they are synchronized. The detailed sensor set-up is shown in Figure 7.

Table 3 lists the regular and irregular wave conditions used during the test. These were adopted from the DOE Wave Energy Prize's tests for 1:30 scale models using Froude scaling [30, 31]. In addition to the wave probe used during testing, two wave probes were used to calibrate the wave before the test to ensure the accuracy of the wave properties. Tests for each wave condition were conducted three times to verify the consistency. It is noticed during the test that the prototype needs a certain amount of time to reach the steady state to provide meaningful data, so for each regular wave the test time is increased to 5 min, and the irregular wave test lasts for 30 min.

4 | RESULTS AND DISCUSSION

The input power absorbed by the point absorber can be presented by:

$$P_m = f_{pto} \dot{z}_{pto} \quad (11)$$

Here f_{pto} is read from the load cell and \dot{z}_{pto} is obtained through the derivation of the displacement acquired from the string pot [32].

In this paper, however, to eliminate the influence of different configurations, the normalized input mechanical power is used

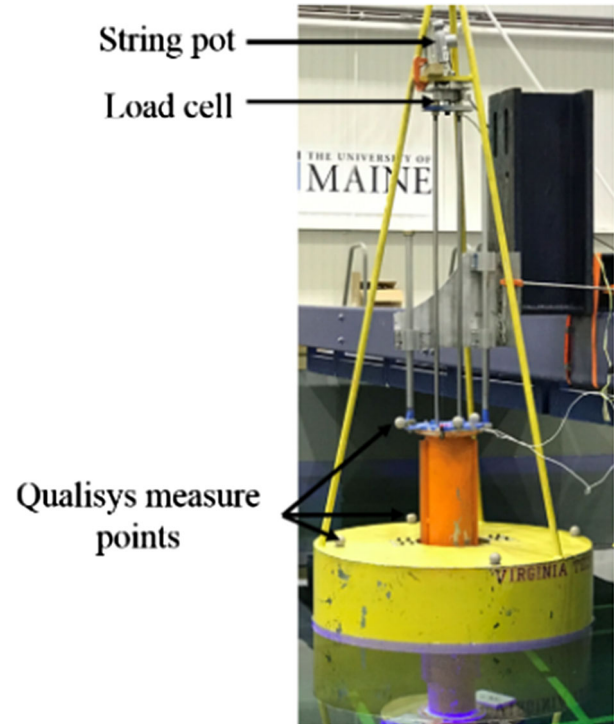


FIGURE 7 Scheme of the sensor set-up

to compare performances by eliminating the influence of different wave height:

$$P_{Norm} = \frac{P_m}{(H_{wave})^2} \quad (12)$$

Figure 8 compares the normalized power between the single body and two-body heave only configurations. For the single body configuration, each case shows the optimal result under the optimal damping coefficient. However, for the two-body heave only configuration, maximum damping coefficient is not achieved due to the limitations of the generator. Although the optimum power of the two-body point absorber is not achieved, Figure 8 shows that the two-body structure still can have better performance, indicating that the two-body design can achieve the frequency tuning effect and that it is reasonable to use a two-body design for better energy absorption [21]. For a more direct comparison, the Capture Width Ratio (CWR) is also illustrated, where the maximum CWR for the two-body configuration can reach almost 60%.

The comparison between the two-body heave-only test and the two-body moored case with the same cone shape submerged body is shown in Figure 9. It can be seen from the figure that the power absorption during the wave tank test are at the same level, however, the moored case has slightly high power. Since the two set-ups are tested under the same damping coefficient, by checking into the time domain simulation, it can be found that the stroke of the relative motion for the two-body heave only case is smaller than the two-body moored case,

TABLE 3 Different wave conditions adopted in the test

Regular wave	Scaled wave period (s)	Scaled wave height (m)	Scaled wave power flux (w/m)	Full scale wave period (s)	Full scale wave height (m)
No.1	2.01	0.079	11.91	11.0	2.36
No.2	2.19	0.094	18.41	12.0	2.81
No.3	2.37	0.110	27.46	13.0	3.30
No.4	2.56	0.128	39.78	14.0	3.83
No.5	2.74	0.146	56.17	15.0	4.39

Irregular wave	Dominant wave period (s)	Significant wave height (m)
No.1	2.83	0.173

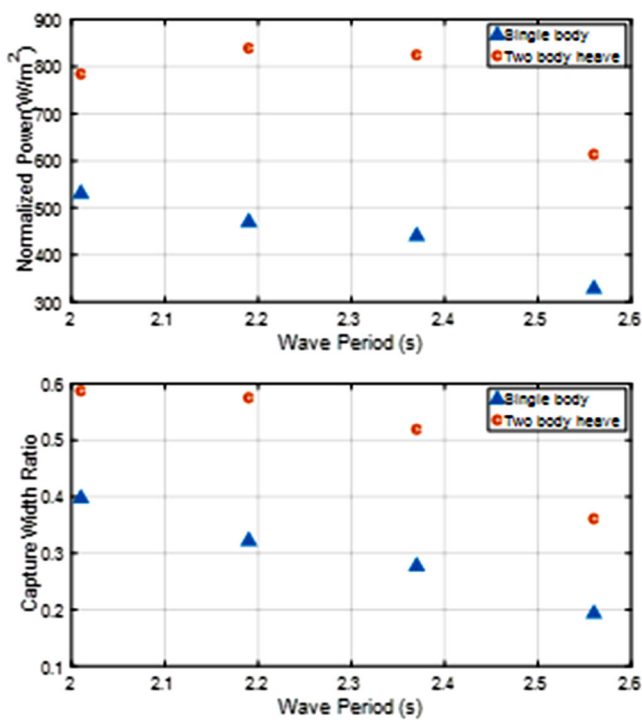


FIGURE 8 Compared test results for the single-body and two-body heave only point absorber: (Top) Normalized power; (Bottom) capture width ratio (CWR)

indicating that the relative heave motion is boosted from the other motions, more specifically, the pitch motion. The regular wave time domain test results can be found in Figure 9 on the right.

In addition to the regular wave, the comparison between the two-body heave only and the moored case in the irregular wave is also explored. A Bretschneider spectrum is adopted to generate the time domain irregular wave profile, and it is formed by the superposition of a series of regular waves with a random phase. The spectrum can be described as:

$$S(\omega) = 0.1687H_s^2\omega_s^{-4}\omega^{-5}\exp(-0.675\omega_s^{-4}\omega^{-4}) \quad (13)$$

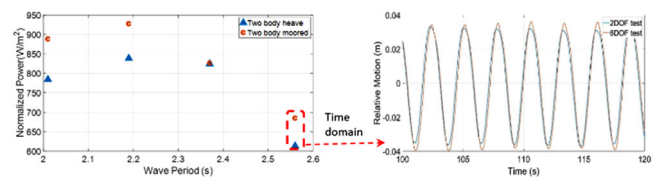


FIGURE 9 (Left) Frequency domain test results for the two-body heave only and two-body moored configuration; (Right) Time domain test results for the indicated case

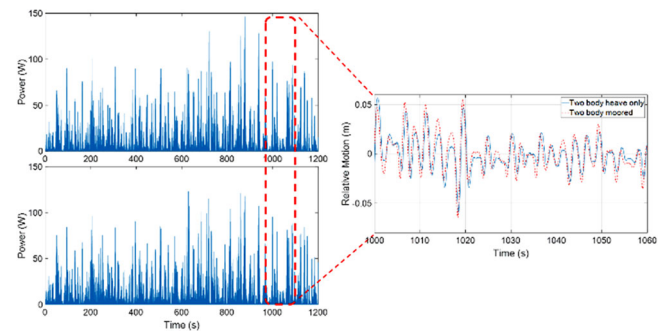


FIGURE 10 (Left top) Two-body heave only configuration irregular wave test results; (Left bottom) Two-body moored configuration irregular wave test results; (Right) Time domain compare for the two cases

Here

- H_s is the significant wave height
- $\omega_s = 2\pi/T_s$, T_s is the significant wave period defined as the average period of the significant waves
- ω is the wave frequency.

The time domain test results of the irregular wave shown in Figure 10 have a similar phenomenon that is observed in the regular ones. The two-body heave only configuration also has a smaller stroke, which leads to a smaller power output. Under the irregular wave with the same time profile, the averaged power absorption for the two-body heave only configuration is 6.42 W with a peak to average ratio of 17.2, whereas the moored con-

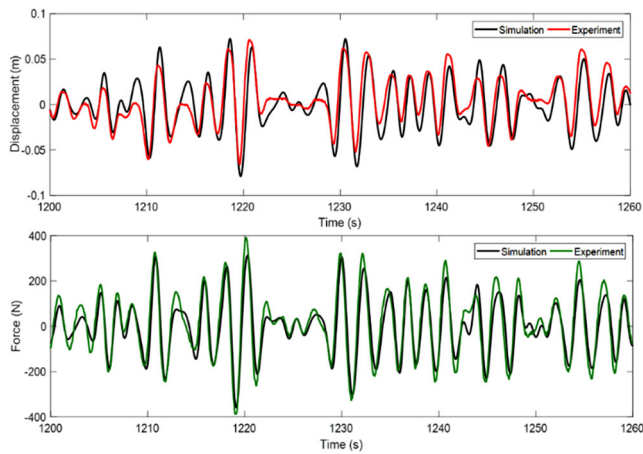


FIGURE 11 Compare of the test results and simulation results for the two-body heave only configuration under irregular wave; (Top) Displacement comparison; (Bottom) PTO force comparison

figuration achieved 7.19 W with a peak to average ratio of 18.0. Proving again that the mooring can benefit the performance of the two-body point absorber.

To verify the accuracy of the dynamic model, the time domain simulation is shown to verify the previously established model. Figure 11 shows the time domain simulation results for the irregular wave case. From the figure, it can be observed that the simulation results match well with the time domain results.

The test results for the different submerged body shape is shown in Figure 12. It can be observed from the figure that the point absorber with a streamlined cone shape second body can achieve better performance. Since both test conditions find the optimum point for the tested configuration, it can be concluded that the heave plate shape design can result in lower

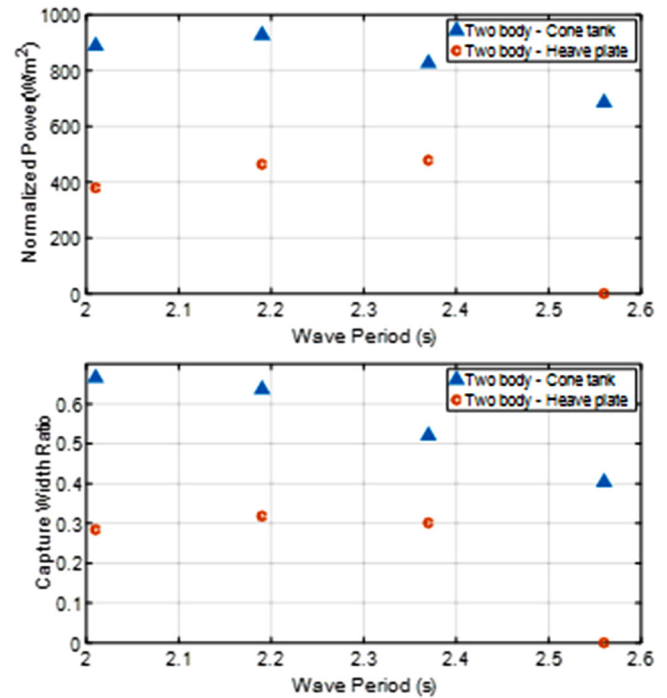


FIGURE 12 Compared test results for the two-body point absorber with different reactive body (Top) Normalized power; (Bottom) CWR

peak power due to the influence of the large drag damping coefficient [33].

Table 4 lists all the configurations and their Capture Width Ratio (CWR) data acquired from the tests. From the table, it can be noticed that the two-body moored case with the cone shape reactive body has the best CWR, which reaches 66.5%, indicating great potential for the two-body point absorber.

TABLE 4 The tested capture width ratio for different configurations with the optimum damping coefficient

Wave condition	Single body	Two body heave only	Two body-cone tank	Two body-heave plate
No.1 (2.01 s, 0.079 m)	39.7	58.7	66.5	28.4
No.2 (2.19 s, 0.094 m)	32.2	57.5	63.6	31.8
No.3 (2.37 s, 0.110 m)	27.7	51.9	52.0	30.1
No.4 (2.56 s, 0.128 m)	19.3	36.1	40.3	—

5 | CONCLUSION AND FUTURE WORK

In this paper, a point absorber type of wave energy converter is analyzed and tested under four different configurations: single-body configuration, two-body heave-only configuration, and two-body moored configurations with different submerged bodies. Dynamic models are established and prototypes were built and tested in wave tanks. Several major conclusions can be drawn from the results.

Firstly, through the two-body reactive structure design, the natural frequency of the point absorber can be successfully adjusted, which brings an advantage in the power absorption.

Secondly, with a reasonable mooring design, the performance of the point absorber can be boosted from the pitch and other motion, thus increasing the overall power absorption.

Moreover, the compared results show that the point absorber can benefit from a more streamlined submerged body shape, the peak performance can be improved by decreasing the drag damping influence.

Lastly, through the explicit characterization of the dynamic model, the numerical simulation can be used as a credible tool for predicting the performance of the point absorber, the dynamic model should be able to predict the performance of a two-body point absorber with acceptable accuracy.

For future work, more complicated mooring configurations will be explored for ocean deployment under different wave conditions. The model can be refined for mooring dynamics and design for the large scale prototypes.

ACKNOWLEDGMENTS

The authors would like to gratefully acknowledge the funding support from the U.S. Department of Energy EERE under Grant No. DE-EE0007174 and the European Union Horizon 2020 Framework Programme (H2020) under grant agreement No. 731084. The authors thank researchers including Dr. Mathew Fowler and Mathew Cameron in Alford W2 Ocean Engineering Lab at the University of Maine and Dr. Francois Petrie at the Oceanide France for help with the wave tank tests.

ORCID

Xiaofan Li  <https://orcid.org/0000-0002-7956-4823>

REFERENCES

- Gunnar, M., et al.: Assessing the global wave energy potential. In: 29th International Conference on Ocean, Offshore and Arctic Engineering: Volume 3. Shanghai, China (2010)
- Nejat, P., et al.: A global review of energy consumption, CO₂ emissions and policy in the residential sector (with an overview of the top ten CO₂ emitting countries). *Renewable Sustainable Energy Rev.* 43, 843–862 (2015)
- Pelc, R., Fujita, R.M.: Renewable energy from the ocean. *Mar. Policy* 26(6), 471–479 (2002)
- Budar, K., Faldes, J.: A resonant point absorber of ocean-wave power. *Nature* 256(5517), 478–479 (1975)
- Evans, D.V.: A theory for wave-power absorption by oscillating bodies. *J. Fluid Mech.* 77(1), 1–25 (1976)
- Mei, C.C.: Power extraction from water waves. *J. Ship Res.* 20, 63–66 (1976)
- Lejerskog, E., et al.: Experimental results on power absorption from a wave energy converter at the Lysekil wave energy research site. *Renewable Energy* 77, 9–14 (2015)
- Sa da Costa, J., et al.: Modeling of an ocean waves power device AWS. In: Proceedings of 2003 IEEE Conference on Control Applications, 2003. CCA. Istanbul, Turkey (2003)
- Vicente, P.C., Falcão, A.F.O., Justino, P.A.P.: Nonlinear dynamics of a tightly moored point-absorber wave energy converter. *Ocean Eng.* 59, 20–36 (2013)
- Wang, L., et al.: Improving electric power generation of a standalone wave energy converter via optimal electric load control. *Energy* 211, 118945 (2020)
- Liu, Y.C., Pastor, J.: Time domain modeling and power output for a heaving point absorber wave energy converter. In: IMECE2014-36374, ASME 2014 International Mechanical Engineering Congress & Exposition. Montreal, Canada (2014)
- Pastor, J., Liu, Y.C.: Power absorption modeling and optimization of a point absorbing wave energy converter using numerical method. *J. Energy Resources Technol.* 136(2), 021207 (2014)
- Pastor, J., Liu, Y.C.: Frequency and time domain modeling & power output for a heaving point absorber wave energy converter. *Int. J. Energy Environ. Eng.* 5(2), 1–13 (2014)
- Guo, B., et al.: Nonlinear modeling and verification of a heaving point absorber for wave energy conversion. *IEEE Trans. Sustainable Energy* 9(1), 453–461 (2017)
- Antonio, F.D.: Wave energy utilization: A review of the technologies. *Renewable Sustainable Energy Rev.* 14(3), 899–918 (2010)
- Faldes, J.: A review of wave-energy extraction. *Mar. Struct.* 20(4), 185–201 (2007)
- Draper, M.: More than just a ripple: Ocean power technologies sets its sights high. *Refocus* 7(1), 54–56 (2006)
- Neary, V.S., et al.: Methodology for Design and Economic Analysis of Marine Energy Conversion (MEC) Technologies. No. SAND2014-3561C. Sandia National Lab (SNL-NM). Albuquerque, New Mexico (2014)
- Weber, J., et al.: Wavebob—research & development network and tools in the context of systems engineering. In: Proceedings of Eighth European Wave and Tidal Energy Conference. Uppsala, Sweden, pp. 416–420 (2009)
- Beatty, S.J., et al.: Experimental and numerical comparisons of self-reacting point absorber wave energy converters in regular waves. *Ocean Eng.* 104, 370–386 (2015)
- Martin, D., et al.: Numerical analysis and wave tank validation on the optimal design of a two-body wave energy converter. *Renewable Energy* 145, 632–641 (2020)
- Xu, Q., et al.: Experimental and numerical investigations of a two-body floating-point absorber wave energy converter in regular waves. *J. Fluids Struct.* 91, 102613 (2019)
- Al Shami, E., Zhang, R., Wang, X.: Point absorber wave energy harvesters: A review of recent developments. *Energies* 12(1), 47 (2018)
- Shek, J.K.H., et al.: Reaction force control of a linear electrical generator for direct drive wave energy conversion. *IET Renewable Power Gener.* 1(1), 17 (2007)
- Ringwood, J.V., Bacelli, G., Fusco, F.: Energy-maximizing control of wave-energy converters: The development of control system technology to optimize their operation. *IEEE Control Syst. Mag.* 34(5), 30–55 (2014)
- Li, X., et al.: A compact mechanical power take-off for wave energy converters: Design, analysis, and test verification. *Appl. Energy* 278, 115459 (2020)
- Armstrong-Hélouvy, B., Dupont, P., De Wit, C.C.: A survey of models, analysis tools and compensation methods for the control of machines with friction. *Automatica* 30(7), 1083–1138 (1994)
- Cummins, W.E.: *The Impulse Response Function and Ship Motions*. David Taylor Model Basin, Washington DC (1962)
- Li, X., et al.: Characterization and verification of a two-body wave energy converter with a novel power take-off. *Renewable Energy* 163, 910–920 (2021)

30. Bull, D., Dallman, A.: Wave energy prize experimental sea state selection. Proceedings of the ASME 2017 36th International Conference on Ocean, Offshore and Arctic Engineering. Volume 10: Ocean Renewable Energy. Trondheim, Norway. <https://doi.org/10.1115/OMAE2017-62675> (2017).
31. Payne, G.: Guidance for the experimental tank testing of wave energy converters. SuperGen Marine. vol. 254. Last accessed March 2021. https://home.hvl.no/ansatte/gste/ftp/MarinLab_files/Litteratur/WEC_tank_testing.pdf (2008).
32. Falnes, J., Kurniawan, A., Ocean Waves and Oscillating Systems: Linear Interactions Including Wave-Energy Extraction. Vol. 8. Cambridge University Press (2020)
33. Yu, Y.-H., Li, Y.: Reynolds-averaged Navier–Stokes simulation of the heave performance of a two-body floating-point absorber wave energy system. Comput. Fluids 73, 104–114 (2013)

How to cite this article: Li, X., et al.: Analysis and wave tank verification of the performance of point absorber WECs with different configurations. IET Renew. Power Gener. 15, 3309–3318 (2021). <https://doi.org/10.1049/rpg2.12253>